An experimental and numerical investigation of buoyancy-driven two-phase displacement

D. E. Weidner and L. W. Schwartz
Department of Mechanical Engineering, The University of Delaware, Newark, Delaware 19716

(Received 20 February 1991; accepted 22 May 1991)

The motion of the interface between two fluids in a Hele–Shaw cell for the case of a cell oriented with the plates vertical is considered. The bottom edge of the cell may be at any angle to the horizontal and only density differences between the two fluids drive the flow. A boundary integral technique is employed to numerically predict the motion of the interface and numerical simulations are compared with experimental results. Unlike pressure-driven Hele–Shaw flow, where the simplified equations predict only qualitative features of the displacement profiles, here the agreement is quite good, in general. Theory predicts and experiment confirms that the displacement profiles are not a function of fluid viscosity.

I. INTRODUCTION

The phenomenon of fingering in Hele–Shaw cells has been studied extensively over the past 30 years. One of the motivations for this interest has been the analogy that exists between the Hele–Shaw equations, which govern the motion of a viscous fluid between two closely separated plates, and Darcy's Law, which governs the motion of fluids in porous media.[1,2] Since laboratory-scale experiments may be readily performed using a Hele–Shaw cell, it has been hoped that theoretical and experimental investigations using the Hele–Shaw cell as a model may be applied toward the solution of many outstanding problems dealing with fluid flow in porous media. One of the most important problems in this class involves secondary oil recovery, in which water or CO_2 is injected into a well to displace oil from the porous medium. Indeed, the same fingering phenomena observed in Hele–Shaw cells appears to occur in oil reservoirs; the latter is thought to limit the recovery of oil from these reservoirs.[3]

One advantage of performing experiments in a Hele–Shaw cell as opposed to using a porous medium stems from the difficulty in observing and recording the motion of a highly contorted two-dimensional interface in a three-dimensional space. The Hele–Shaw cell avoids this problem by geometrically constraining the third dimension, thereby giving time-dependent, two-dimensional curves, which may be readily recorded. For the case of a cell oriented with its plates perpendicular to gravity, experimental and theoretical results could be extrapolated to predict the motion of fluids in a porous medium in those cases where only horizontal motions were of importance.

Here we investigate the motion of two fluids in a Hele–Shaw cell when the plates of the cell are oriented vertically; hence the density difference between the two fluids is incorporated in the equations of motion. In particular we consider the case of the cell oriented as shown in Fig. 1, where one fluid (air) has a negligible density and viscosity in comparison to the second fluid (usually castor oil). The cell is oriented at any angle α to the horizontal, and only density differences between the air and the viscous liquid drive the flow. The reason for considering such a cell lies in the simplicity of its construction and operation in comparison to an open-ended cell driven by a constant pressure or injection rate pump. In addition, a direct analogy exists between this geometry and the hydrologic problem of gravity-driven flow in tilted strata.[4] In a related experiment,[5] Maxworthy measured several averaged characteristics of the interface in a gravity-driven cell for $\alpha = \pi/2$. Greenkorn *et al.*[6] previously considered a cell with a similar geometry with $\alpha = 0$, but they used a constant pressure pump with an open-ended cell. Their analytical method ignored surface tension, contributing, no doubt, to the large discrepancy between their experimental observations and their numerically predicted displacement profiles. We employ a boundary integral method, which includes the effects of surface tension, and find good agreement between our experimental results and numerical predictions. In Sec. II the equations of motion are derived and the problem is nondimensionalized. In Sec. III we give details of the boundary integral technique and discuss its numerical implementation. The construction and operation of our experimental cell is described in Sec. IV. Experimental and numerical results are discussed in Sec. V.

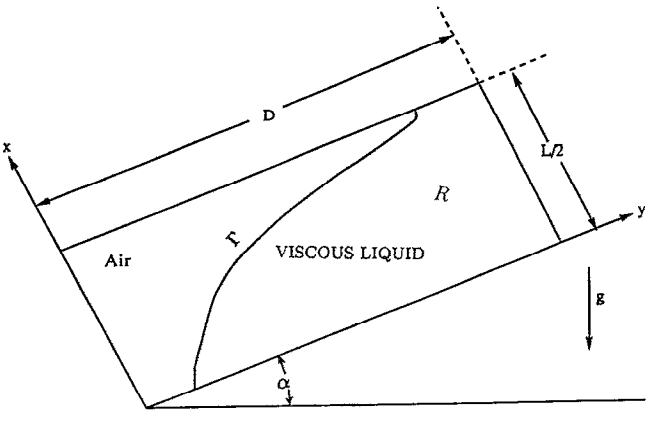

FIG. 1. Hele–Shaw cell oriented with the plates parallel to gravity and the long axis of the cell at angle α to the horizontal. The two plates are separated by a distance b (into page).

 0899-8213/91/092076-05$02.00

II. FORMULATION

Consider the cell shown in Fig. 1. It is of finite length D, width $L/2$, plate spacing b, and is oriented at angle α to the horizontal. The pressure in the liquid region R is a function of the spatial coordinates x and y. The depth-averaged velocity is related to the pressure gradient according to

$$\mathbf{v} = -M\nabla p, \tag{1}$$

where M, the mobility, equals $b^2/12\mu$. On the moving boundary Γ, p includes a hydrostatic component given by

$$p_s = \rho g(x\cos\alpha + y\sin\alpha). \tag{2}$$

In the liquid region, the hydrostatic pressure does not influence the velocity field and will be omitted. Incompressibility yields

$$0 = \nabla\cdot\mathbf{v} = \nabla^2 p. \tag{3}$$

The air has negligible viscosity and density compared to the viscous liquid, and may be assumed to be at zero pressure. The pressure jump across the air–liquid interface Γ is given by

$$p(x,y) = \sigma[(1/R_\perp) + (1/R_\parallel)] \quad [(x,y)\in\Gamma], \tag{4}$$

where σ is the surface tension, $R_\parallel$ is the radius of curvature in the plane of the cell, and $R_\perp$ is the radius of curvature in the direction perpendicular to the parallel plates. Following previous authors,[1,2] $R_\perp$ is assumed constant for this problem. This leads to the following pressure condition on the moving boundary:

$$p(x,y) = \sigma\frac{d\theta}{ds} \quad [(x,y)\in\Gamma], \tag{5}$$

where θ is the angle a tangent to the interface makes with respect to some reference direction and s is the arclength along the interface. Hence $d\theta/ds = 1/R_\parallel$, and the constant contribution to p, arising from $R_\perp$, has been ignored. Viewed from the liquid side of the interface, p is positive when the surface is concave. The pressure on the moving boundary reduces to

$$p(x,y) = \sigma\frac{d\theta}{ds} + \rho g(x\cos\alpha + y\sin\alpha) \quad [(x,y)\in\Gamma]. \tag{6}$$

On the solid walls of the cell at $x = 0$, $x = L/2$, and $y = D$, the boundary condition of no normal flow is

$$\nabla p(x,y)\cdot\hat{\mathbf{n}} = 0, \tag{7}$$

where $\hat{\mathbf{n}}$ is a unit normal. Note that at $y = 0$ there is no boundary condition since by hypothesis the liquid is never allowed to reach the left end of the cell. The no-slip boundary conditions at the top, bottom, and right edge of the cell cannot be imposed within the constraints of the Hele–Shaw model.

The problem is made dimensionless by usng L, $L/\rho gM$, and ρgL as units of length, time, and pressure, respectively. The pressure field p satisfies Laplace's equation within the liquid region while on Γ it is given by

$$p(x,y) = \tau\frac{d\theta}{ds} + x\cos\alpha + y\sin\alpha \quad [(x,y)\in\Gamma], \tag{8}$$

where τ, the dimensionless surface tension, is given by

$$\tau = \sigma/\rho gL^2. \tag{9}$$

Once the pressure field is known, the interface may be marched in time according to

$$\mathbf{v} = -\nabla p(x,y). \tag{10}$$

For a given Hele–Shaw cell of length D with a fixed angle of inclination to the horizontal α, the *shape* of the curves generated in the cell from some given initial state is a function only of τ. Note that a cell with flow driven by a pump,[2] the succession of profiles depend on both μ and b, but here it depends on neither.

III. SOLUTION TECHNIQUES

As in an earlier work,[2] where a similar problem was solved without the effect of gravity, the moving boundary will be represented by a line source distribution $q(s)$. This method, justified by the results of potential theory,[7] makes it possible to find the velocities at all points along the interface curve as well as points within the liquid domain R.

In order to deal with the boundary condition at $x = 0.5$, an image source line is introduced. This curve is the reflection of the actual interface curve about the top edge of the cell; by making the source strength magnitudes along this curve identical to the magnitudes of the sources assigned to the actual interface curve, the requirement of no flow through this wall is satisfied. The actual interface is now confined between $x = 0$ and $x = 0.5$, while the top image is between $x = 0.5$ and $x = 1$. The bottom edge boundary condition ($x = 0$) is satisfied by use of the conformal mapping

$$\zeta = e^{2\pi iz}. \tag{11}$$

Note that this mapping takes the line representing the end of the cell $y = D$ in the z plane into a circle centered at the origin of radius

$$r^{(\zeta)} = e^{-2\pi D} = a. \tag{12}$$

The actual interface curve with its upper image in the z plane is transformed into a closed symmetric curve lying outside of this circle. (See Fig. 2.) Through the use of this mapping, the top boundary is mapped onto the positive η axis, and, by symmetry, the boundary condition of no flow through the bottom of the cell is automatically satisfied.

Since the mapping is analytic, Laplace's equation remains the governing equation in the region between the outer closed curve and the circle $r^{(\zeta)} = a$ with the boundary condition $\partial p/\partial n = 0$ on the circle.

Let p be the real part of the complex potential $f(\zeta)$. The complex velocity in the $\zeta = \xi + i\eta$ plane is

$$u^{(\zeta)} - iv^{(\zeta)} = \frac{df}{d\zeta} = \frac{df}{dz}\frac{dz}{d\zeta}, \tag{13}$$

where $u^{(\zeta)}$ and $v^{(\zeta)}$ are the velocities in the ξ and η directions, respectively.

The circle theorem[8] gives the system of images necessary to make the circle $r^{(\zeta)} = a$ a streamline. The circle theorem requires the placement of an elemental source of strength dQ inside the circle at $\zeta = a^2e^{i\theta}/b$ for every source of strength dQ outside the circle at $\zeta = be^{i\theta}$, and a sink of strength $-dQ$ at the center. Hence the complex potential in

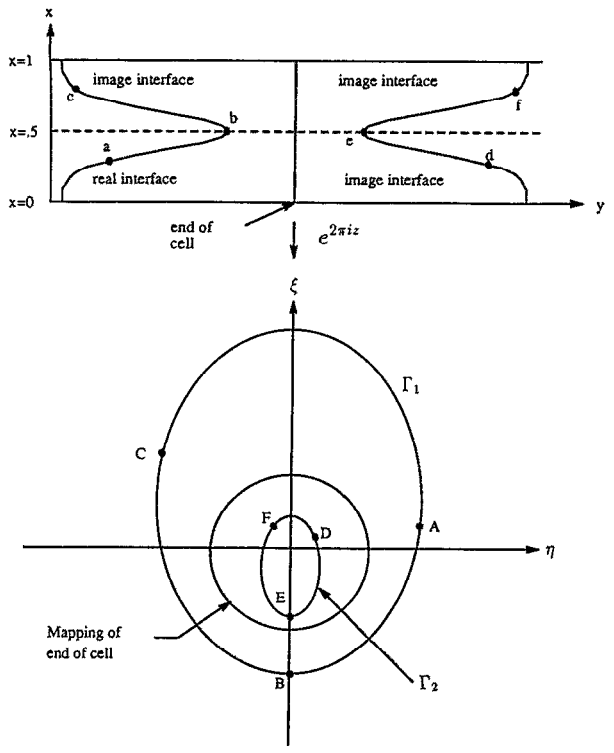

FIG. 2. The interface and its image system in the (x,y) and (η,ξ) planes. Corresponding points are indicated by upper and lowercase letters.

the closed region between the circle $r^{(\xi)} = a$ and Γ_1 is the sum of three integrals;

$$f(\zeta) = \frac{1}{2\pi}\oint_{\Gamma_1} q(s_1)\ln(\zeta-\zeta_1)ds_1 + \frac{1}{2\pi}\oint_{\Gamma_2} q(s_2)\ln(\zeta-\zeta_2)ds_2 - \frac{1}{2\pi}\ln\zeta\oint_{\Gamma_1} q(s_1)ds_1, \tag{14}$$

where ζ_1, ds_1, and ζ_2, ds_2 denote values on Γ_1 and Γ_2, respectively, as in Fig. 2.

Symmetry in the z plane implies

$$q(s_2) = q(s_1)\left|\frac{ds_1}{ds_2}\right| \tag{15}$$

and

$$\zeta_2 = \zeta_1|\zeta_1|^{-2}e^{-4\pi D}. \tag{16}$$

Equating the real part of (14) to $p(s_1)$ yields

$$\int_{\Gamma_1} q(s_1)\ln\left|\frac{(\zeta-\zeta_1)(\zeta-\zeta_2)}{\zeta}\right|ds_1 = 2\pi p(s_1). \tag{17}$$

Once $q(s_1)$ is known (13) is used to determine the velocity in the mapped plane,

$$u^{(\xi)} - iv^{(\xi)} = \frac{1}{2\pi}\int_{\Gamma_1}\left(\frac{1}{(\zeta-\zeta_1)} + \frac{1}{(\zeta-\zeta_2)} - \frac{1}{\zeta}\right)q(s_1)ds_1 - i\frac{q(s_1)}{2}e^{-i\beta}, \tag{18}$$

where β is the slope of the curve, measured counterclockwise from the direction of increasing $\mathrm{Re}(\zeta)$. The velocity of the boundary points in the z plane can be found by

$$\frac{d\bar{z}}{dt} = \frac{df}{dz} = \frac{df}{d\zeta}\frac{d\zeta}{dz} \quad (\zeta\in\Gamma_1), \tag{19}$$

where $\bar{z} = x - iy$.

The interfacial curve in the z plane is discretized into $n+1$ nodes, where the first node is located at the intersection of the interface with the top of the cell, and the $(n+1)$th node is at the intersection of the interface with the cell bottom. At any instant of time, the potential p at these nodes is calculated using a discrete version of Eq. (8). After mapping the nodes to the ζ plane, the potentials at the midpoints, between the nodes, are determined by interpolation. The source distribution is taken to be piecewise constant and the integrals in Eqs. (17) and (18) are discretized.[9] The resulting linear system for the source distribution from (17) is solved and the ζ-plane velocities are calculated from (18). After interpolation back to the nodes, the velocities are transformed to the z plane using (19).

Given the node positions at any time and finding the corresponding particle velocities by the above procedure, the surface coordinates are found as the solution of a coupled system of first-order nonlinear ordinary differential equations. These are solved using the LSODE[10] package. In order to maintain adequate resolution as the interface evolved, the nodes were periodically redistributed along a cubic-spline representation of the interface and additional nodes were added as the interface lengthened. Runs were repeated using more nodes until convergence under refinement was established.

IV. EXPERIMENTAL SETUP AND OPERATION

The experimental cell consisted of two rectangular glass plates separated by strips of rubber that act both as spacers as well as defining the upper and lower edges of the cell and the right (enclosed) end. Each glass plate is 0.63 cm thick, and the rectangular region between the rubber seals measures 80 cm long by 10.18 cm wide. Twelve C clamps were attached to a wood framework surrounding the outside perimeter of the cell to maintain a uniform plate spacing of 0.15 cm. This wood framework was bolted to a wood block that was secured to a stand designed to hold the cell at any angle to the horizontal. (See Fig. 3.)

Initially, the long edge of the cell was oriented vertically ($\alpha = -90°$) and the cell was filled with a liquid to a depth of 50 cm. Then the cell was rotated to a set angle to the horizontal and the evolving shape of the interface was recorded using both a 35 mm camera and a video camera. A digital stop watch was mounted to the side of the cell.

Several liquids were used in the cell, including castor oil and various dilutions of glycerin. Castor oil was found to be the best fluid due to its superior wetting properties against glass. The interfacial curve between castor oil and air was always smooth, while the curve between the glycerin and air sometimes showed irregularities. The viscosity of castor oil is quite temperature dependent; hence the predicted variation of finger speed with μ could be confirmed by running

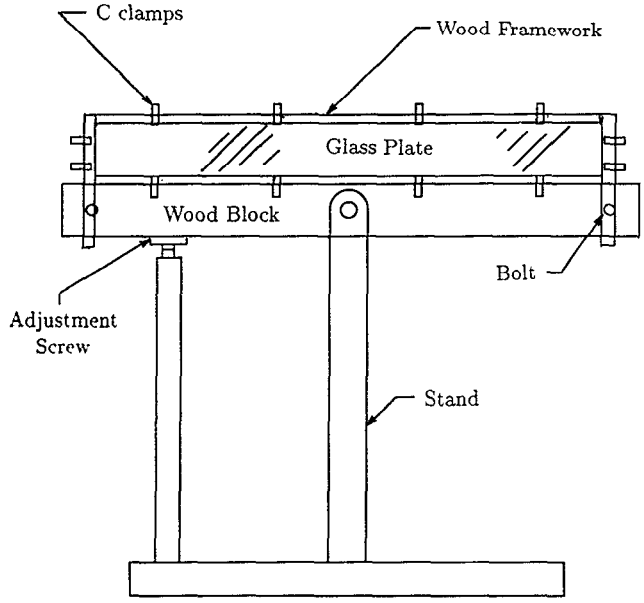

FIG. 3. The experimental cell.

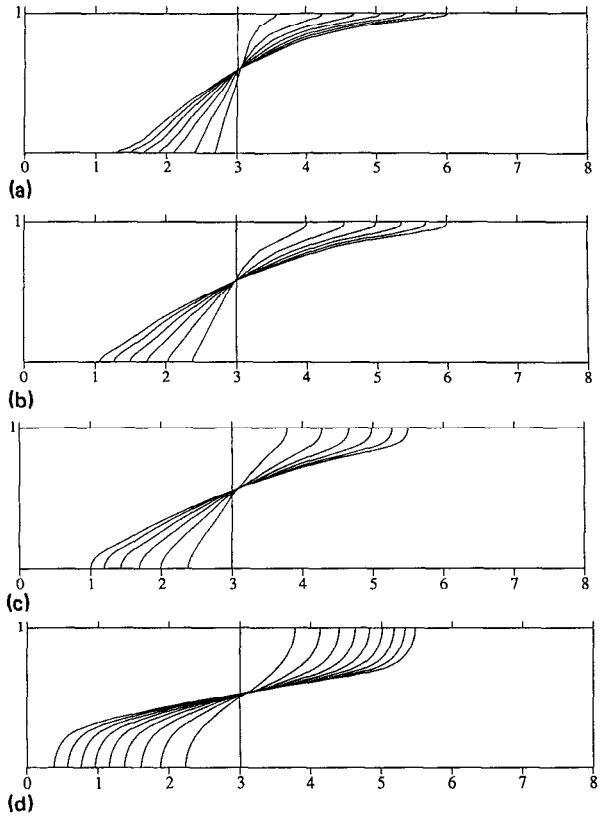

FIG. 4. Numerically generated interfacial profiles for different values of the nondimensional surface tension τ. The initial interface is a vertical line at $y = 3$ and the x coordinate has been magnified by a factor of 2. (a) $\tau = 10^{-5}$, $\Delta t = 0.11$; (b) $\tau = 10^{-4}$, $\Delta t = 0.18$; (c) $\tau = 10^{-3}$, $\Delta t = 0.3$; and (d) $\tau = 10^{-2}$, $\Delta t = 0.5$.

the experiment at different temperatures. The temperature of the castor oil in the cell was measured before and after each experimental run using a Keithley model 871 digital thermocouple thermometer. Viscosities were found using a Brookfield Model DV-I digital viscometer. The values for density and surface tension, which are weakly dependent on temperature (less than 1% variation in the temperature range considered), were obtained from a standard handbook.[11]

V. EXPERIMENTAL AND NUMERICAL RESULTS

Figure 4 shows the numerically generated finger profiles for a horizontal cell ($\alpha = 0$) for τ values between 10^{-5} and 10^{-2}. In each case, the interface begins as a vertical line at $y = 3$ and the sequence of profiles shown represent equal spacings in t. Note that not only does the finger become "rounder" with increasing τ, but the profiles become more symmetric with respect to the initial configuration.

Figure 5 shows the evolving interfacial curves for castor oil at two different temperatures (symbols □ and △, respectively) as well as the numerical prediction (solid line) for a horizontal cell. By raising the temperature of castor oil from 17 °C to 23 °C, the viscosity is lowered from 13 P to 8 P while the surface tension and density remain essentially unchanged. The dimensionless surface tension for this experimental arrangement is $\tau = 1.0 \times 10^{-4}$. The shapes of the experimental curves for the two trials are predicted to be identical, while the speeds of the moving interface should differ by a factor of 0.62. In fact, the speed difference between the two runs was a factor of 0.61; Fig. 5 demonstrates the expected similarity in finger shape for the two experimental runs, as well as good agreement with the numerical simulation.

Figure 6 shows an enlargement of Fig. 5(b) at the leading edge of the finger, near the top edge of the cell. The Hele–Shaw model requires that the interface intersect the top of the cell wall at an angle of 90°, while the experimental meniscus is observed to "roll" along the upper rubber seal of the cell at an angle approaching 180°. The discrepancy between experimental observations and numerical predictions in this

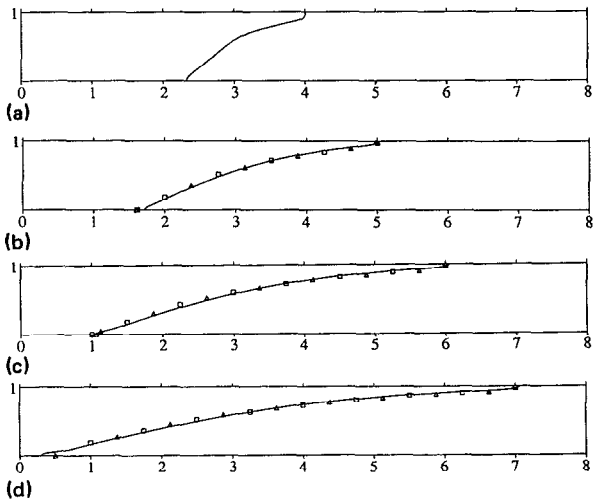

FIG. 5. Comparison of numerically predicted interfacial profiles, at various times, with experimental results, for $\alpha = 0$. The cell is filled with castor oil.—, numerical ($\tau = 1.0 \times 10^{-4}$); □, $\mu = 8$ P (23 °C); △, $\mu = 13$ P (17 °C). (a) $t = 0$, (b) $t = 0.36$, (c) $t = 0.9$, and (d) $t = 1.6$.

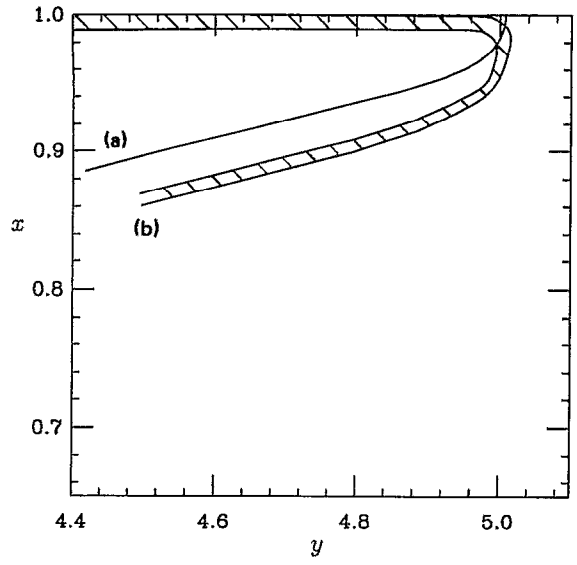

FIG. 6. Enlargement of Fig. 5(b) near the top edge of the cell. (a) numerical; (b) experimental; $\mu = 13$ P. Illustration of the local deviation from the Hele–Shaw model.

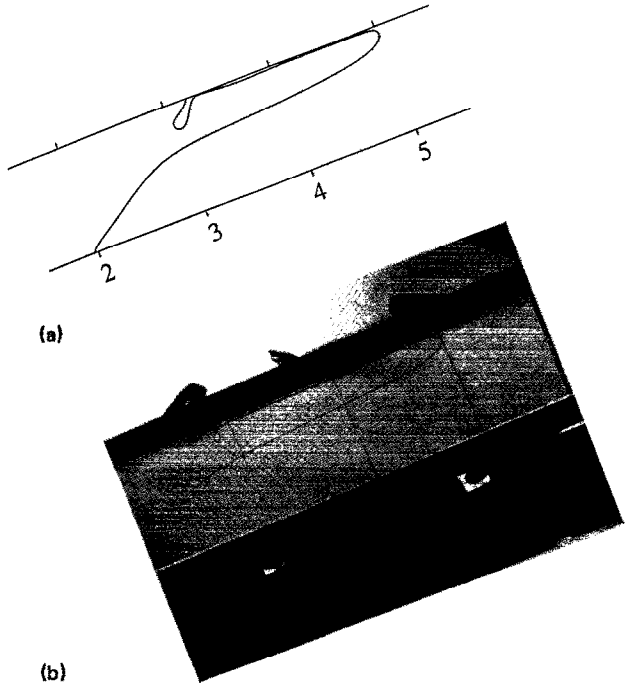

FIG. 7. (a) Numerically generated interfacial profile; $\alpha = \pi/4$, $\tau = 1.0 \times 10^{-4}$. (b) Photograph of the experimental cell.

region is due to two factors: (1) the no-slip boundary condition at the cell edges cannot be enforced within the context of the Hele–Shaw theory; and (2) the numerically generated interface profile is a one-dimensional curve, whereas the experimentally observed meniscus between the castor oil and the air is approximately $b/2$ thick.

Figure 7(a) shows the numerically generated finger profiles for a cell oriented at $\alpha = \pi/4$ with $\tau = 10^{-4}$, while Fig. 7(b) is a photograph of the experimental cell operating with the same parameters. Note the presence of the liquid drop at the top edge of the cell behind the advancing finger, and the fact that the simulation qualitatively captures this effect.

It is remarkable that, apart from the immediate neighborhood of the cell edges, the simplified Hele–Shaw theory is quantitatively valid. This may be contrasted with pressure-driven "fingering" flows, where the steady-state finger width is consistently underpredicted.[1,12,13] While improved results for pressure-driven flows may be obtained by use of local capillary-number-dependent corrections,[14,15] it is clear that the simple theory lacks important elements of the relevant physics. The success of the theory in the present case is associated, no doubt, with the absence of explicit dependence on capillary number.

ACKNOWLEDGMENT

This work was partially supported by the National Science Foundation under Grant No. MSM-8707856.

[1] P. G. Saffman and G. I. Taylor, Proc. R. Soc. London Ser. A **245**, 312 (1958).
[2] A. J. De Gregoria and L. W. Schwartz, J. Fluid Mech. **164**, 383 (1986).
[3] L. W. Schwartz and A. J. DeGregoria, J. Aust. Math. Soc. **29**, 375 (1988).
[4] C. M. Marle, *Multiphase Flow in Porous Media* (Gulf, Paris, 1981).
[5] T. Maxworthy, J. Fluid Mech. **177**, 207 (1987).
[6] A. L. Greenkorn, J. E. Mater, and R. C. Smith, AIChE J. **13**, 273 (1964).
[7] M. A. Jaswon and G. T. Symm, *Integral Equation Methods in Potential Theory and Elastostatics* (Academic, New York, 1977).
[8] L. M. Milne-Thomson, *Theoretical Hydrodynamics* (MacMillan, New York, 1968).
[9] J. F. Botha and G. F. Pinder, *Fundamental Concepts in the Numerical Solution of Differential Equations* (Wiley, New York, 1983).
[10] A. C. Hindmarsh, *Livermore Solver for Ordinary Differential Equations (LSODE)* (Lawrence Livermore Laboratory, Livermore, CA, 1980).
[11] *Handbook of Chemisry and Physics*, edited by R. C. Weast (CRC Press, Cleveland, OH, 1977).
[12] J. W. McLean and P. G. Saffman, J. Fluid Mech. **102**, 445 (1981).
[13] J. M. Vanden-Broeck, Phys. Fluids **26**, 2033 (1983).
[14] L. W. Schwartz, Phys. Fluids **29**, 3086 (1986).
[15] L. W. Schwartz and A. J. DeGregoria, Phys. Rev. A **35**, 276 (1987).